Inverse-kinematics one-neutron pickup with fast rare-isotope beams

A. Gade,[1,2] J. A. Tostevin,[3,4] T. Baugher,[1,2] D. Bazin,[1] B. A. Brown,[1,2] C. M. Campbell,[1,*] T. Glasmacher,[1,2] G. F. Grinyer,[1,†] S. McDaniel,[1,2] K. Meierbachtol,[1,5] A. Ratkiewicz,[1,2] S. R. Stroberg,[1,2] K. A. Walsh,[2] D. Weisshaar,[1] and R. Winkler[1]

[1]*National Superconducting Cyclotron Laboratory, Michigan State University, East Lansing, Michigan 48824, USA*

[2]*Department of Physics and Astronomy, Michigan State University, East Lansing, Michigan 48824, USA*

[3]*Department of Physics, Faculty of Engineering and Physical Sciences, University of Surrey, Guildford, Surrey GU2 7XH, United Kingdom*

[4]*Department of Physics, Tokyo Institute of Technology, 2-12-1 Ookayama, Meguro-ku, Tokyo 152-8550, Japan*

[5]*Department of Chemistry, Michigan State University, East Lansing, Michigan 48824, USA*

(Received 28 September 2010; revised manuscript received 7 March 2011; published 31 May 2011)

Measurements and reaction model calculations are reported for single-neutron pickup reactions onto a fast ^{22}Mg secondary beam at 84 MeV per nucleon. Measurements made on both carbon and beryllium targets, having very different structures, were used to investigate the likely nature of the pickup reaction mechanism. The measurements involve thick reaction targets and γ-ray spectroscopy of the projectile-like reaction residue for final-state resolution, which permit experiments with low incident beam rates compared to traditional low-energy transfer reactions. From measured longitudinal momentum distributions we show that the ^{12}C(^{22}Mg, ^{23}Mg $+\gamma$)X reaction largely proceeds as a direct two-body reaction, with the neutron transfer producing bound ^{11}C target residues. The corresponding reaction on the ^{9}Be target seems to largely leave the ^{8}Be residual nucleus unbound at excitation energies high in the continuum. We discuss the possible use of such fast-beam one-neutron pickup reactions to track single-particle strength in exotic nuclei and also their expected sensitivity to neutron high-ℓ (intruder) states, which are often direct indicators of shell evolution and the disappearance of magic numbers in the exotic regime.

DOI: 10.1103/PhysRevC.83.054324 PACS number(s): 25.60.Je, 24.50.+g, 24.10.−i, 27.30.+t

I. INTRODUCTION

The spectroscopy and ordering of nucleon single-particle levels along extended isotopic chains is of importance for understanding emerging and dissolving shell structures. One- and two-nucleon removal reactions from fast rare-isotope beams are making a significant contribution to such studies in some of the rarest isotopes [1–3]. This information, in turn, allows an assessment of shell-model effective interactions and of their predictions near both the weakly and strongly bound Fermi surfaces in highly neutron-proton asymmetric nuclei. By their nature these nucleon removal reactions preferentially populate states in the heavy residual nuclei with a strong hole-like parentage upon the projectile ground state. For the spectroscopy of particle-like states, light-ion single-nucleon transfer reactions, such as the (d,p) reaction, are very often the reaction of choice. These reactions are best and most often carried out at relatively low incident energies such that linear and angular momentum matching and hence the reaction yields are optimal. The beam intensity, (thin) target, and detection system demands for such measurements, of final-state-resolved transfer cross section angular distributions in inverse kinematics, are however high and such studies remain impractical, currently, for many of the most exotic nuclei.

In this paper we consider test case measurements and associated direct reaction model calculations for reaction events in which a single neutron is picked up by a fast secondary beam of mass A. The measurements employ thick targets and γ-ray spectroscopy and thus take full advantage of fast beams produced by fragmentation; the resulting high luminosity allows for experiments with low incident beam rates [4]. Related previous studies [5,6] considered reactions involving the pickup of a strongly bound proton from a ^{9}Be target. Here we discuss measurements for a ^{22}Mg beam of about 84 MeV per nucleon incident energy. An important aspect of the present analysis is that measurements are made using both carbon and beryllium reaction targets, with very different neutron structures. Two of our primary aims here are to investigate (a) the nature of the fast pickup reaction mechanism and (b) the magnitudes of the measured and calculated pickup reaction yields. In doing so we hope to gain some insight into the potential to use such reactions, in combination with γ-ray spectroscopy of the populated mass $A+1$ final states, to determine quantitative particle state spectroscopy information on exotic nuclei produced at energies of order 100 MeV per nucleon. Specifically, we aim to clarify whether the reaction proceeds predominantly by a direct single-particle pickup mechanism and, if this is the case, to quantify the measured and calculated cross sections for transfers involving different orbital angular momenta ℓ. Such information will illustrate, for instance, the capability for future measurements to identify high-ℓ neutron intruder components in the low-energy spectra of the pickup residues. Since such high-ℓ intruder configurations are typically angular momentum mismatched, they are more weakly coupled and populated in lower energy (d,p) transfer reactions.

*Present address: Nuclear Science Division, Lawrence Berkeley National Laboratory, Berkeley, California 94720, USA.

†Present address: Grand Accélérateur National d'Ions Lourds (GANIL), CEA/DSM-CNRS/IN2P3, Bvd Henri Becquerel, 14076 Caen, France.

We make clear in advance that the fast nucleon pickup events considered here are not well matched in either transferred linear or angular momentum, in the sense used in semiclassical model discussions of transfer reactions between heavy ions [7,8]. We also make clear that the ^{23}Mg residues in the present analysis, having a high first nucleon threshold, do not permit a detailed or quantitative spectroscopy in this case. Our aims here are more modest and were stated above. In addition, to help direct future experiments, we assess the effectiveness of our two light target choices: (a) ^{12}C, which makes available four well-bound $p_{3/2}$ neutrons with a ground-state separation energy of $S_n = 18.72$ MeV, and (b) ^{9}Be, which offers one weakly bound valence neutron of $S_n = 1.665$ MeV, while $S_{2n} > 20$ MeV, in providing a source of neutrons with sufficiently high momentum components to contribute strength to the pickup reaction yields. We will show that the measured and calculated pickup reaction yields and the ^{23}Mg residue momentum distributions measured on the two targets help to provide such a clarification and guide to future studies.

II. EXPERIMENTAL DETAILS

The projectile beam of ^{22}Mg was obtained by fragmentation of a 170-MeV per nucleon ^{24}Mg primary beam provided by the Coupled Cyclotron Facility at the National Superconducting Cyclotron Laboratory (NSCL) on the campus of Michigan State University. The ^{9}Be fragmentation target of 1904 mg/cm^2 thickness was located at the midacceptance target position of the A1900 fragment separator [9]. An achromatic aluminum wedge degrader of 600 mg/cm^2 thickness and slit systems were used to purify the beam. The momentum acceptance of the separator was restricted to $\Delta p/p = 0.14\%$. The resulting cocktail beam of $N = 10$ isotones contained ^{22}Mg (74%), ^{21}Na (24.5%), and ^{20}Ne (1.5%).

Targets of 188 mg/cm^2 thick ^{9}Be and 149.4 mg/cm^2 thick ^{nat}C (vitreous carbon with a density of $\rho = 1.54$ g/cm^3, 98.9% enriched in ^{12}C) were placed at the reaction target position of the S800 spectrograph [10] to induce the one-neutron pickup onto the ^{22}Mg projectiles. The target position was surrounded by the high-resolution γ-ray detection system SeGA, an array of 32-fold segmented high-purity germanium detectors [11]. The high degree of segmentation allows for event-by-event Doppler reconstruction of the γ rays emitted by the projectile-like reaction residues in flight. The angle of the γ-ray emission entering the Doppler reconstruction is determined from the location of the segment that registered the largest energy deposition. The photopeak efficiency of the detector array was calibrated with standard sources and corrected *in-beam* for the Lorentz boost of the γ-ray distribution emitted by nuclei moving at $v/c > 0.35$.

Event-by-event particle identification was performed with the focal-plane detection system [12] of the large-acceptance S800 spectrograph. The energy loss measured with the S800 ionization chamber and time-of-flight information taken between plastic scintillators, corrected for the angle and momentum of each ion, were used to unambiguously identify the projectile-like reaction residues exiting the target.

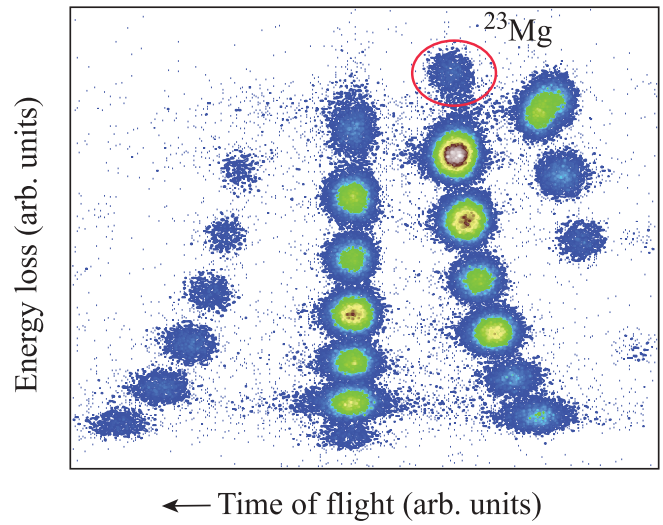

FIG. 1. (Color online) Particle identification spectrum (energy loss vs time of flight) for ^{23}Mg produced in the ^{12}C(^{22}Mg, ^{23}Mg + γ)X one-neutron pickup reaction. The spectrum shows all projectile-like reaction residues from the interaction of ^{22}Mg with the C target that entered the S800 focal plane in the same magnetic rigidity setting as ^{23}Mg.

The incoming projectiles were identified from their flight-time difference measured with plastic timing detectors. The particle-identification spectrum for ^{23}Mg produced in ^{22}Mg + ^{12}C is shown in Fig. 1.

For each target, the inclusive cross section for the one-neutron pickup to all bound final states of ^{23}Mg was determined from the yield of detected pickup residues divided by the number of incoming projectiles relative to the number density of the ^{9}Be and ^{12}C reaction targets, respectively. The γ-ray spectra observed in coincidence with ^{23}Mg, event-by-event Doppler reconstructed, are displayed in Fig. 2. Partial cross sections to individual final states were obtained from the efficiency-corrected full-energy peak areas relative to the number of pickup products and corrected for feeding. Unfortunately, the statistics were not sufficient to tag the final state of the ^{11}C target nuclei in the laboratory-frame γ-ray spectra ($v/c \approx 0$).

Position information from the two cathode readout drift chambers (CRDCs) of the S800 focal-plane detection system together with trajectory reconstruction employing the optics code COSY [13] was used to reconstruct the longitudinal momentum distributions of the pickup residues on an event-by-event basis. Figure 3 shows for both the Be and the C targets the momentum distributions of the pickup product ^{23}Mg together with the momentum profile of the ^{22}Mg beam passing through the target essentially unreacted. The width of the ^{22}Mg momentum profile as measured in the spectrograph's focal plane is dominated by the energy (momentum) straggling of the projectiles in the respective reaction target. The curves through the data points are to guide the eye and have been used in the case of the ^{23}Mg distributions to determine acceptance corrections on the low-momentum side of 9.9% and 5% for the cross sections measured with the Be and C targets, respectively. The widths of the ^{23}Mg momentum

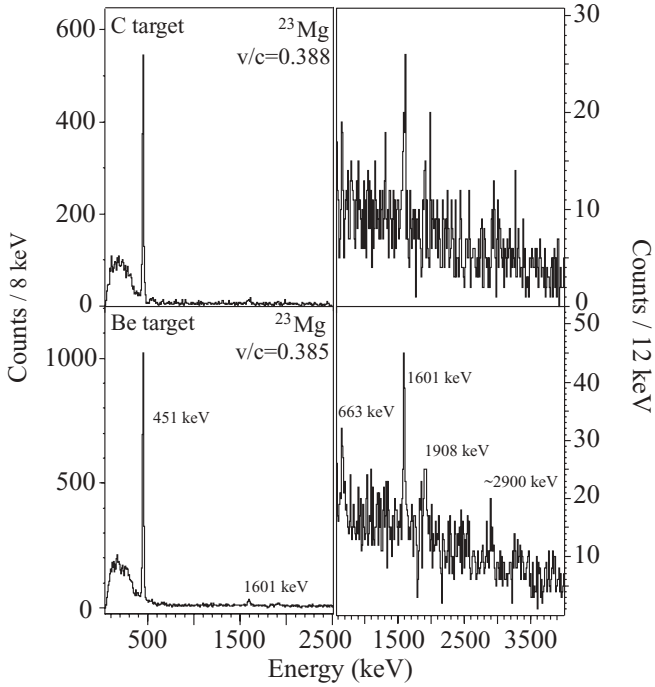

FIG. 2. Event-by-event Doppler reconstructed γ-ray spectra measured in coincidence with ^{23}Mg populated in ^{12}C(^{22}Mg, ^{23}Mg + γ)X (top) and ^{9}Be(^{22}Mg, ^{23}Mg + γ)X (bottom), respectively. Left: The prominent γ-ray transition at 451 keV depopulates the $5/2^+_1$ excited state to the $3/2^+$ ground state; right: expansion of the higher energy part of the γ-ray energy spectrum. The other γ rays correspond to transitions from the known $7/2^+$, $1/2^+$, and $9/2^+$ or $5/2^+$ excited states at 2052, 2359, and 2715 keV [14], respectively. There is some indication of a transition at about 2900 keV, which may depopulate the alleged $(3/2, 5/2)^+$ state at 2908 keV excitation energy [14].

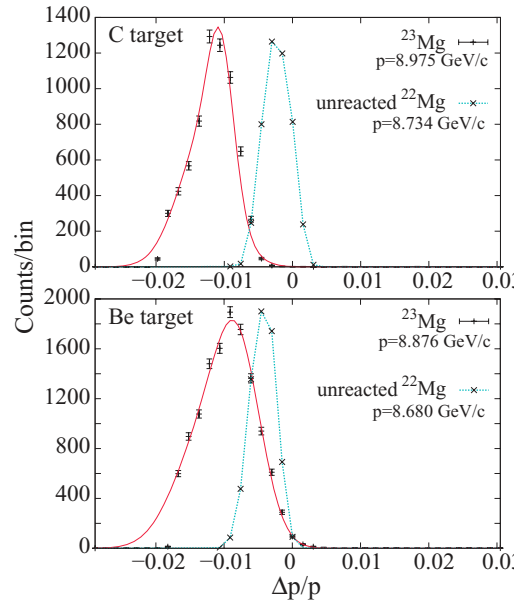

FIG. 3. (Color online) Momentum distributions of the one-neutron pickup product ^{23}Mg and momentum profile of the ^{22}Mg projectile beam passing through the Be and C targets, respectively. The lines are to guide the eye and have been used for the ^{23}Mg distribution to estimate acceptance losses on the low-momentum side caused by a beam blocker in the S800 focal plane that was necessary to prevent the direct beam from entering the detection system.

distributions are strikingly different for the measurements with the two different targets while the momentum profiles of the unreacted ^{22}Mg projectiles are essentially identical in both cases. The differential momentum loss δp of ^{23}Mg that takes into account that the pickup can, with equal probabilities, occur at any point along the trajectory through the target was found to be negligible ($\delta p/p < 1.8 \times 10^{-3}$), unlike in the case of one-proton pickup [5]. Figure 4 shows the measured angular distributions of the heavy residues as a function of their laboratory-frame angle, $d\sigma/d\theta_L$, for the pickup reactions induced by both targets. The spectra demonstrate that essentially the entire final-state distributions and yield are within the spectrograph's angular acceptance.

If the neutron pickup reaction is strictly *two body*, i.e., it involves only transfers between bound states of the target and the projectile and also leaves a bound target-like residue, then the intrinsic, reaction-mechanism-induced parallel momentum distribution of the heavy projectile-like residues, $d\sigma/dp_\parallel$, will be very narrow. The necessary formula is given by Eq. (1) of Ref. [5]. So, unlike knockout reaction measurements, the residue momentum distribution does not provide spectroscopic (orbital angular momentum) information; however, it carries a reaction mechanism diagnostic, as follows.

Following strict two-body transfers, the intrinsic $d\sigma/dp_\parallel$ momentum distribution is essentially δ-function-like in comparison to the incident beam momentum resolution $\Delta p/p \approx 0.14\%$ and the energy broadening due to passage through the target. Thus, the extent to which the measured ^{23}Mg residue momentum distribution differs from that of the unreacted ^{22}Mg beam provides direct evidence for events that go beyond a two-body reaction model description. We note that this direct comparison of the measured ^{23}Mg distributions from the carbon and beryllium targets with that of the unreacted ^{22}Mg, shown in Fig. 3, leads to qualitatively different outcomes in the two cases. We return to this important point in discussions of the calculated and measured cross sections.

III. REACTION MODEL CALCULATIONS

We consider the neutron-pickup reactions to be described by a post form, fully-finite-range, coupled channels Born approximation (CCBA) reaction analysis. The neutron pickup from the light target(s) is assumed to take place in a single step and we include transfers to ^{22}Mg in its ground and first excited 2^+ state. We carry out these CCBA calculations using the flexible direct reactions code FRESCO [15].

The (all-order) inelastically coupled 0^+ and 2^+ ^{22}Mg core states and the single-step transfer channel paths included in our calculations are shown in Fig. 5. The ^{23}Mg bound states populated by neutron capture onto the ^{22}Mg(2^+) core, which all involve a $1d_{5/2}$ orbital, are represented by dashed lines. We note that the proton threshold in ^{23}Mg is at $S_p = 7.58$ MeV, and thus only the strongest low-lying shell-model states have been

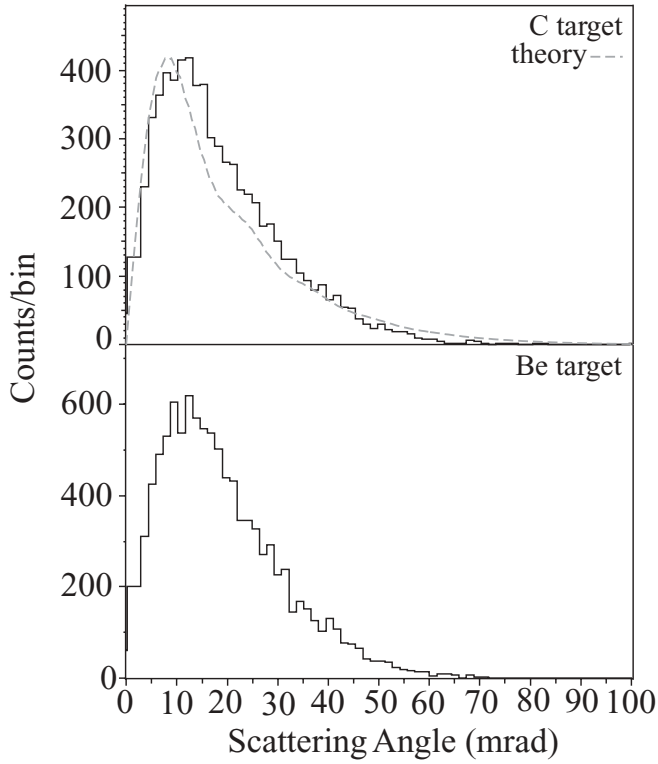

FIG. 4. Laboratory-frame scattering-angle distribution, $d\sigma/d\theta_L$, of the heavy residues measured in the experiment for the carbon (upper panel) and the beryllium (lower panel) targets. For the carbon target a calculated laboratory-frame angular distribution is also shown (dashed curve) for pickup to a single final state, the 0.451 MeV, $5/2^+$ state (with ^{11}C left in its $3/2^-$ ground state). The latter curve has been scaled to the measurements to aid comparison of the shapes but does not take into account small folding effects due to the finite emittance of the incident beam and from angular straggling in the target. The spectra show that the distributions fit well into the elliptical angular acceptance of the S800 spectrograph ($\pm 5^\circ \times \pm 3.5^\circ$) in agreement with the calculations.

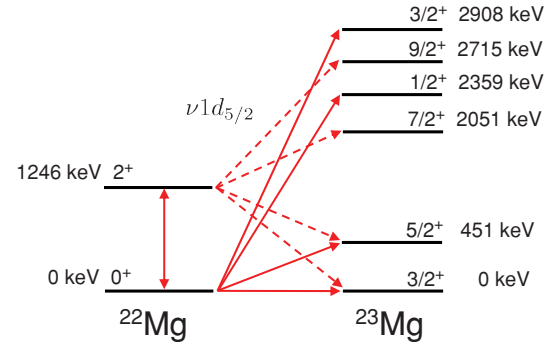

FIG. 5. (Color online) Schematic of the CCBA channel-coupling scheme used for the ^{22}Mg(^{12}C,^{11}C)^{23}Mg(J^π) and ^{22}Mg(^{9}Be,^{8}Be*)^{23}Mg(J^π) neutron pickup reactions. The solid lines (from ^{22}Mg to ^{23}Mg) represent one-step single-particle transfers to the final states indicated. The dashed lines show two-step pathways to ^{23}Mg states, by neutron capture onto the ^{22}Mg(2^+) core. All of these involve a $1d_{5/2}$ neutron orbital.

included in Fig. 5. The shell model also predicts fragmented sd-shell strength to states up to the proton threshold that will be quantified, approximately, later. The entrance and exit channel distorting optical model interactions used and our treatment of the ^{22}Mg projectile excitation are also discussed later.

We first consider the possible implications of the light target nucleus structures on our reaction treatment. We note that our two-body CCBA reaction methodology assumes kinematics and dynamics in which the projectile and target in the initial and final states separate as two bound systems. The neutron is assumed to be transferred from bound states in the target to bound states in the projectile residue, with the target residue remaining bound. For the carbon target case our expectation is that this two-body picture will be an excellent approximation (for either neutron or proton pickup). Here we make use of the ^{12}C ($=^{11}$C $+ n$) structure information as was deduced for the corresponding neutron knockout reactions from ^{12}C, as discussed in Ref. [16]. The ground-state neutron separation energy is $S_n = 18.72$ MeV and neutron pickup will leave the ^{11}C residue predominantly in its ground state ($3/2^-$) or the excited states at 2.000 ($1/2^-$) and 4.804 MeV ($3/2^-$). These three states lie well below the first ^{11}C threshold of 8.69 MeV. Theoretically the shell-model spectroscopic factors to these three states, calculated with the Warburton and Brown p-shell (WBP) interaction [17], are $C^2S = 3.16$, 0.58, and 0.19 and are seen to essentially exhaust the four units of single-particle strength expected. The very small remainder, of 0.07, is fragmented over numerous ^{11}C states above 10 MeV in excitation. These WBP interaction spectroscopic factors agree well with other p-shell shell-model calculations and thus this description of the ^{12}C target is robust.

We also take from Ref. [16] the ^{11}C $+ n$ Woods-Saxon binding potential geometry used to calculate these p-shell neutron overlaps. These have radius and diffuseness parameters of 1.310 and 0.55 fm, respectively. A ^{11}C (^{12}C) root mean squared (rms) matter radius of 2.12 (2.32) fm was assumed for the calculation of the ^{11}C + ^{23}Mg (^{12}C + ^{22}Mg) distorting potentials, as described below.

For the ^{9}Be target the situation is significantly more complex. The configurations of the single weakly bound valence neutron, with $S_n = 1.665$ MeV, relative to the unbound (but near the two-α-particle threshold) ^{8}Be 0^+ and 2^+ states have been studied in some detail. The associated neutron overlaps and their spectroscopic factors from the variational Monte Carlo (VMC) wave functions of Wiringa and coworkers [18,19] and from extended microscopic cluster model wave functions, e.g., Arai *et al.* [20], are in rather close agreement. In both cases the $[0^+ \otimes p_{3/2}]_{3/2}$ and $[2^+ \otimes p_{3/2}]_{3/2}$ configurations are completely dominant. The cluster model (VMC) spectroscopic factors for these two configurations are 0.553 (0.591) and 0.514 (0.583), respectively. In the following we use the numerical ^{8}Be 0^+ and 2^+ core state overlaps from Arai *et al.* [21] (as are shown in Fig. 4(a) of Ref. [20]).

For convenience, these overlaps were fitted to single-particle wave functions calculated in Woods-Saxon potential wells, with separation energies of 1.665 and 4.695 MeV. The fitted reduced radius, r_0, diffuseness, a_0, and spin-orbit strength parameters, V_{so}, written $(r_0, a_0)V_{so}$ were (1.09 fm, 0.59 fm) 6.0 MeV and (1.09 fm, 0.75 fm) 6.0 MeV in the two

cases. As will be discussed further, the amplitudes for valence neutron pickup will leave the target-like residues unbound and resonant (though only very weakly so). However, if the reaction proceeds by the pickup of a more strongly bound neutron (from the ^{8}Be core) the resulting target residues will be left at high excitation in the continuum; this core-state single-particle strength is in the vicinity of 15 MeV of excitation in ^{8}Be*. We noted already the qualitative difference between the measured momentum distributions of the ^{23}Mg residues from reactions on the beryllium and carbon targets. These and the cross sections presented below indicate that such core neutron pickup events are dominant in the case of the ^{9}Be target and hence that our two-body dynamical model is not appropriate for a quantitative discussion of fast pickup reaction yields in this case.

Concentrating first on the ^{12}C case, we compute the pickup reaction as ^{22}Mg[^{12}C,^{11}C(I^{π})]^{23}Mg(J^{π}), leading to the $I^{\pi} = 3/2^{-}_{1}$, $1/2^{-}$, and $3/2^{-}_{2}$ states of ^{11}C at 84 MeV per nucleon incident energy. The (absorptive) nuclear optical interactions were calculated, as is done in the fast nucleon knockout reaction studies, by double folding the neutron and proton densities of ^{22}Mg (^{23}Mg), obtained from spherical Skyrme (SkX interaction) Hartree-Fock (HF) calculations [22], and of ^{12}C (^{11}C), assumed a Gaussian with rms radius given earlier, with an effective nucleon-nucleon (NN) interaction [23]. The ^{22}Mg was allowed to inelastically excite (Fig. 5) by deforming the entrance channel nuclear distorting potential with a deformation length of $\delta_2 = 1.95$ fm. This corresponds to an assumed mass β_2 value of 0.58, consistent with the charge β_2 of 0.58(11) from Ref. [24]. The binding geometry and spectroscopic factors of the $^{11}\mathrm{C} + n$ overlaps were already detailed above.

The required neutron-projectile bound states and overlaps $[^{22}\mathrm{Mg}(0^{+}, 2^{+}) \otimes n\ell_j]_J$ and their spectroscopic amplitudes were taken from full sd-shell shell-model calculations that use the recently rederived USDB, Universal sd-shell Hamiltonian of Brown and Richter [25]. As is indicated in Fig. 5, there are interfering paths for population of the ^{23}Mg($3/2^{+}$) ground state, via the $[0^{+} \otimes 1d_{3/2}]$ and $[2^{+} \otimes 1d_{5/2}]$ transfers. Both of these paths are weak in the present case, resulting in a small predicted ^{23}Mg ground-state cross section. The first excited $5/2^{+}$, 451-keV state is also shown to proceed by both direct and indirect, 2^{+} state, paths. However, this calculated $[2^{+} \otimes 1d_{5/2}]$ USDB spectroscopic factor is 0.005, so this (negligible) two-step path is not considered further. The state at 2.715 MeV, shown in the literature as $9/2^{+}$, $(5/2^{+})$, is assumed in our calculations to be a $9/2^{+}$ state, and it can be associated with a large-amplitude $[2^{+} \otimes 1d_{5/2}]_{9/2}$ core-coupled shell-model state at 2.762 MeV. There is no shell-model candidate for a $5/2^{+}$ state near this energy.

The USDB shell-model spectroscopic factors C^2S are collected in Tables I and II. The associated single-particle states were calculated in real Woods-Saxon potential wells, all with diffuseness parameter $a_0 = 0.7$ fm and a spin-orbit interaction of strength 6 MeV. The reduced radius parameters r_0 of these potentials were adjusted to reproduce the rms radius of each single-particle orbital, as given by the same Hartree Fock calculations as were used to calculate the projectile densities, as has been discussed in detail elsewhere [26]. These r_0 values were 1.284, 1.315, and 1.134 fm for the $1d_{5/2}$, $1d_{3/2}$, and $2s_{1/2}$ orbitals, respectively. These overlap functions were calculated using their physical separation energies, computed from the ground-state separation energy, $S_n = 13.15$ MeV, and the excitation energies. The theoretical reaction yields for the carbon target are collected in Table I. These are shown summed with respect to the three ^{11}C final states and which are dominated, because of the large spectroscopic factor, by the ground-state contribution. The cross sections are computed by integrating the calculated center-of-mass frame differential cross sections for angles $\theta_{\mathrm{c.m.}} < 40^{\circ}$. At this upper angle limit the cross sections have fallen to 10^{-9} of their values at forward angles.

Calculations in the ^{9}Be target case were identical as far as the projectile-like system is concerned. Regarding the target, the neutron pickup was computed as due only to the weakly bound valence neutron, i.e., ^{22}Mg[^{9}Be,^{8}Be(0^{+}, 2^{+})]Mg(J^{π}). The summed spectroscopic strength to these two ^{8}Be final states is of order unity. The nuclear distorting interactions were

TABLE I. Experimental cross sections compared to the CCBA reaction and shell-model calculations for the fast single-neutron pickup reactions ^{22}Mg[^{12}C,^{11}C(I^{π})]^{23}Mg(J^{π}) at 84 MeV per nucleon. The theoretical cross section σ^{th} is inclusive with respect to the population of the $I^{\pi} = 3/2^{-}$, $1/2^{-}$, and $3/2^{-}$ states of the ^{11}C target residue. The spectroscopic amplitudes of the interfering $[0^{+} \otimes 1d_{3/2}]$ and $[2^{+} \otimes 1d_{5/2}]$ ground-state paths have the same sign.

J^{π}	E (keV)	σ_f expt. (mb)	Configuration SM	C^2S SM	σ^{th} (mb)
$3/2^{+}$	0.0	$\leqslant 0.77^{+0.09}_{-0.13}$	$[0^{+} \otimes 1d_{3/2}]$	0.054	0.083
			$[2^{+} \otimes 1d_{5/2}]$	0.939	
$5/2^{+}$	451	1.27(14)	$[0^{+} \otimes 1d_{5/2}]$	0.410	1.448
$7/2^{+}$	2051	0.18(5)	$[2^{+} \otimes 1d_{5/2}]$	0.574	0.054
$1/2^{+}$	2359	0.08(5)	$[0^{+} \otimes 2s_{1/2}]$	0.242	0.010
$9/2^{+}$	2715	0.10(5)	$[2^{+} \otimes 1d_{5/2}]$	0.366	0.096
$3/2^{+}$	2908	–	$[0^{+} \otimes 1d_{3/2}]$	0.238	0.326
inclusive cross section: 2.40(19) mb					

TABLE II. Experimental cross sections compared to the CCBA reaction and shell-model calculations for the fast single-neutron pickup reactions ^{22}Mg[^{9}Be,^{8}Be(I^{π})]^{23}Mg(J^{π}) at 84 MeV per nucleon. The theoretical cross section σ^{th} is inclusive with respect to the population of the $I^{\pi} = 0^{+}$ and 2^{+} states of the ^{8}Be target residue. The spectroscopic amplitudes of the interfering $[0^{+} \otimes 1d_{3/2}]$ and $[2^{+} \otimes 1d_{5/2}]$ ground-state paths have the same sign.

J^{π}	E (keV)	σ_f expt. (mb)	Configuration SM	C^2S SM	σ^{th} (mb)
$3/2^{+}$	0.0	$\leqslant 0.86^{+0.08}_{-0.11}$	$[0^{+} \otimes 1d_{3/2}]$	0.054	0.010
			$[2^{+} \otimes 1d_{5/2}]$	0.939	
$5/2^{+}$	451	1.32(12)	$[0^{+} \otimes 1d_{5/2}]$	0.410	0.206
$7/2^{+}$	2051	0.15(4)	$[2^{+} \otimes 1d_{5/2}]$	0.574	0.006
$1/2^{+}$	2359	0.13(4)	$[0^{+} \otimes 2s_{1/2}]$	0.242	0.003
$9/2^{+}$	2715	0.13(4)	$[2^{+} \otimes 1d_{5/2}]$	0.366	0.010
$3/2^{+}$	2908	–	$[0^{+} \otimes 1d_{3/2}]$	0.238	0.037
inclusive cross section: 2.58(16) mb					

calculated by assuming Gaussian ^{9}Be and ^{8}Be matter densities both with rms radius of 2.36 fm. The ^{22}Mg deformation was treated as for the carbon target case. The binding geometry and spectroscopic factors of the $^{8}\mathrm{Be} + n$ overlaps were detailed above, taken from the model of Arai *et al.* [20]. The theoretical reaction yields are collected in Table II, where they are summed with respect to the two ^{8}Be final states.

IV. RESULTS AND DISCUSSION

The $^{12}\mathrm{C}(^{22}\mathrm{Mg}, ^{23}\mathrm{Mg} + \gamma)X$ one-neutron pickup reaction was performed at 84.7 MeV per nucleon mid-target energy. The longitudinal momentum distribution of the ^{23}Mg residues, reconstructed in the focal plane of the S800 spectrograph [see Fig. 3 (top)], was cut by the spectrograph's beam blocker, necessary to stop the direct ^{22}Mg beam passing through the target. A 5% correction for the missing counts was applied to the cross section. The inclusive cross section, including the acceptance correction, amounts to $\sigma_{\mathrm{inc}} = 2.40(19)$ mb. A 6% systematic uncertainty, attributed to fluctuations in the incoming beam composition, was added in quadrature to the statistical uncertainty. From the γ-ray spectra taken in coincidence with the ^{23}Mg reaction products, the partial cross sections for the population of the $5/2^{+}_{1}$, $7/2^{+}_{1}$, $1/2^{+}_{1}$, and the proposed $9/2^{+}$, $5/2^{+}$ levels at 451, 2052, 2359, and 2715 keV, respectively, were obtained from the intensity of the observed γ-ray transitions and the known feeding patterns. Known transitions that were not observed in the present experiment due to limited statistics or γ-ray detection efficiency, for example the 2359-keV ground-state transition of the first $1/2^{+}$ state, are included in our partial cross sections by using the reported branching ratios in the literature [14]. The partial cross section for the $3/2^{+}$ ground state was derived from the inclusive cross section by subtraction of all observed feeders. The possible population of the $(3/2, 5/2)^{+}$ state at 2.9 MeV is included in the uncertainty. We stress that, due to possible unobserved feeding by higher energy γ-ray transitions, the ground-state cross section, in particular, should be considered an upper limit. The measured cross sections are summarized in Table I where they are compared to calculations.

The results for the calculation of the carbon-induced reaction are expected to be reliable, quantitatively. The momentum distribution comparison made in Fig. 3 provides evidence that the reaction proceeds as a direct neutron transfer reaction producing *bound* ^{11}C residues. The calculated cross sections track the values and trends of the measurements reasonably accurately, the exception being the larger experimental yield recorded against the ground-state transition (i.e., all reaction events without an identifiable γ ray). As was stated earlier, the present ^{23}Mg final-state case is very challenging, with the proton decay threshold only at 7.58 MeV. As seen from Table I, the USDB shell-model calculation predicts a state with appreciable $[0^{+} \otimes 1d_{3/2}]$ strength near a known $(5/2,\ 3/2)^{+}$ state at 2.908 MeV with a calculated cross section of 0.33 mb. This state was not clearly identified in the current experiment; however, by assuming that the peak structure in the γ-ray spectra at 2900 keV is the ground-state transition of this state, the partial cross section for its population is estimated to be around 0.2 mb. Similarly, the shell model predicts a summed $[0^{+} \otimes 1d_{5/2}]$ strength of 0.64 to final states up to 8 MeV in excitation in ^{23}Mg. Only 0.41 of this strength has been accounted for in the 451-keV $5/2^{+}$ state, which is responsible for a calculated cross section of 1.45 mb. It is likely therefore that there is a population of fragmented d-wave states with a summed direct reaction cross section yield near that recorded against the ground state, $0.77^{+0.09}_{-0.13}$ mb. This value should thus be considered as an upper limit and an estimate of these direct populations of unobserved fragmented states, which decay by energetic γ rays. In the present case, in addition to the sd-shell shell-model states discussed, there may also be unobserved contributions from bound $f_{7/2}$ fragments at higher excitation energy. The present experiment and data set show no evidence for and do not allow any meaningful discussion of such configurations.

The $^{9}\mathrm{Be}(^{22}\mathrm{Mg}, ^{23}\mathrm{Mg} + \gamma)X$ one-neutron pickup reaction was performed at 84.2 MeV per nucleon mid-target energy. The inclusive cross section was measured for several data runs and found to be constant within the statistical uncertainty. Since for this target the longitudinal momentum distribution of the ^{23}Mg residues is much wider than for the carbon-target-induced reaction [see Fig. 3 (bottom)], the low-momentum tail of the distribution is cut more severely by the beam blocker. A 9.9% correction for the missing counts was applied to the cross section. The inclusive cross section, including the acceptance correction and with a 6% systematic uncertainty added, amounts to $\sigma_{\mathrm{inc}} = 2.58(16)$ mb. The γ-ray spectra and population patterns for the carbon- and beryllium-induced reactions are very similar. In fact, the partial cross sections are identical within uncertainties. Again, the partial cross section for the $3/2^{+}$ ground state was obtained by subtracting the populations from all observed feeders, with the possible population of the $(3/2, 5/2)^{+}$ state at 2.9 MeV included in the uncertainty. In addition, due to possible unobserved feeding by higher energy γ-ray transitions, the ground-state cross section is expected to be an upper limit. The measured cross sections are summarized in Table II and discussed below.

The results for the ^{9}Be target allow us to draw some immediate conclusions. The cross sections in Table II, calculated by assuming pickup only of the valence neutron, are considerably smaller than those measured. This result, combined with the similarity of the measured values to those of the carbon target and the (non-two-body) width of the measured ^{23}Mg momentum distribution for this target (see Fig. 3), points to the dominance of reaction events involving the pickup of strongly bound neutrons from ^{9}Be. We conclude that the momentum composition of the wave function of the weakly bound neutron does not match effectively the needs of the fast pickup mechanism. As was discussed earlier, the strength associated with the core neutrons is located at ^{8}Be excitation energies high in the continuum, near and in excess of 15 MeV, and so it cannot be modeled quantitatively within the CCBA framework. It is interesting to observe that empirically these four neutrons in the (two-α-particle) ^{8}Be core contribute approximately the same cross sections, state-by-state, as the carbon target (see Table I).

It can be deduced from Table I that the fast pickup reaction is also selective in populating the states with higher orbital angular momentum transfer. In the present experiment our

ability to probe this aspect of the reaction is limited since only s- and d-wave neutron final states are resolved. The $[0^+ \otimes 1d]$ configurations are seen to dominate. However, we can begin to clarify this expected orbital angular momentum sensitivity using our theoretical CCBA calculations for the carbon target. To make transparent this ℓ sensitivity, without the need to remove spectroscopic factors and Q-value considerations, we calculated the pickup cross sections for assumed $2s_{1/2}$, $1p_{3/2}$, $1d_{5/2}$, and $1f_{7/2}$ transfers, all with unit spectroscopic factor and with all states located at the position of the physical 0.451-MeV state, and so with separation energy 12.70 MeV. The summed (over ^{11}C final states) single-particle cross sections obtained are $\sigma_{sp} = 0.04$, 0.58, 3.51, and 11.12 mb, respectively. These values represent real enhancements with ℓ, due to improved linear and angular momentum matching, above those due to the advantageous $2J + 1$ final-state multiplicative factor. This is clear from the rescaled values $\sigma_{sp}/(2J + 1) = 0.02$, 0.116, 0.585, and 1.39 mb, respectively. This suggests that there is the potential for this reaction mechanism to help locate emerging particle strength associated with high-ℓ intruder orbitals that enter the low-energy levels spectrum of rare nuclei.

V. CONCLUDING COMMENTS

In summary, measurements and reaction model calculations are presented for the fast one-neutron pickup reactions ^{12}C(^{22}Mg, ^{23}Mg $+ \gamma)X$ and ^{9}Be(^{22}Mg, ^{23}Mg $+ \gamma)X$ at mid-target energies of about 84 MeV per nucleon. Measurements were made using both carbon and beryllium targets, having distinctly different neutron single-particle configurations. Significant differences in the widths of the ^{23}Mg longitudinal momentum distributions for the two different targets were observed, pointing to the differences in the corresponding reaction mechanisms. These data thus provide evidence that the ^{12}C(^{22}Mg, ^{23}Mg $+ \gamma)X$ reactions proceed largely as a direct neutron transfer—producing ^{11}C target residues in bound states—while the corresponding pickup reactions induced by ^{9}Be appear to leave the ^{8}Be target-like residue highly excited and in the continuum.

Partial cross sections to ^{23}Mg final states are calculated (inclusive with respect to the target residue final states) based on the coupled channels Born approximation and assuming shell-model configurations for the ^{23}Mg final states. These cross sections are in reasonable quantitative agreement with the measured excited state partial cross section values. Clearly these pickup partial cross sections in themselves provide insufficient information to determine empirically both the dominant single-particle transferred angular momentum and their spectroscopic strengths—and must be used in conjunction with structure theory. Based on our observed (theoretical) sensitivity of the fast pickup reactions to high-momentum components in the nuclear wave function and the ℓ of the transferred nucleon, we propose their possible application in helping to map the descent of high-ℓ neutron single-particle (intruder) states in regions of shell evolution where traditional neutron magic numbers break down. Specifically, we envisage that the fast pickup mechanism could be used, together with theoretical predictions of level ordering and spectroscopic factors, to study the systematics of and test level migration predictions along isotopic chains, thereby providing an assessment of shell-model and effective interaction predictions. This could provide complementary information to transfer reaction studies, where these overlap, and potentially extend measurements into regions currently inaccessible (by virtue of beam intensity) to transfer. Examples are the most neutron rich Ne, Na, and Mg isotopes approaching $N = 20$, where the neutron intruder $f_{7/2}$ orbital is lower in energy and dominates ground-state and low-lying configurations in the "Island of Inversion" [27].

ACKNOWLEDGMENTS

The authors would like to thank Dr. Koji Arai for providing tables of the overlaps, from Fig. 4(a) of Ref. [20], expressed with conventional shell-model spin couplings. This work was supported by the National Science Foundation under Grants No. PHY-0606007 and No. PHY-0758099 and by the UK Science and Technology Facilities Council (STFC) through Research Grant No. ST/F012012. JAT gratefully acknowledges the financial and facilities support of the Department of Physics, Tokyo Institute of Technology.

[1] P. G. Hansen and J. A. Tostevin, Annu. Rev. Nucl. Part. Sci. **53**, 219 (2003).
[2] A. Gade *et al.*, Phys. Rev. Lett. **99**, 072502 (2007).
[3] P. Adrich *et al.*, Phys. Rev. C **77**, 054306 (2008).
[4] A. Gade and T. Glasmacher, Prog. Part. Nucl. Phys. **60**, 161 (2008).
[5] A. Gade *et al.*, Phys. Rev. C **76**, 061302(R) (2007).
[6] A. Gade *et al.*, Phys. Lett. B **666**, 218 (2008).
[7] D. Brink, Phys. Lett. B **40**, 37 (1972).
[8] W. R. Phillips, Rep. Prog. Phys. **40**, 345 (1977).
[9] D. J. Morrissey *et al.*, Nucl. Instrum. Methods Phys. Res. B **204**, 90 (2003).
[10] D. Bazin *et al.*, Nucl. Instrum. Methods Phys. Res. B **204**, 629 (2003).
[11] W. F. Mueller *et al.*, Nucl. Instrum. Methods Phys. Res. A **466**, 492 (2001).
[12] J. Yurkon, D. Bazin, W. Benenson, D. J. Morrissey, B. M. Sherrill, D. Swan, and R. Swanson, Nucl. Instrum. Methods Phys. Res. A **422**, 291 (1999).
[13] M. Berz, K. Joh, J. A. Nolen, B. M. Sherrill, and A. F. Zeller, Phys. Rev. C **47**, 537 (1993).
[14] National Nuclear Data Center [http://www.nndc.bnl.gov/].
[15] I. J. Thompson, Computer code FRESCO. Available at [http://www.fresco.org.uk/index.htm]. See also I. J. Thompson, Comput. Phys. Rep. **7**, 167 (1988).
[16] B. A. Brown, P. G. Hansen, B. M. Sherrill, and J. A. Tostevin, Phys. Rev. C **65**, 061601 (2002).
[17] E. K. Warburton and B. A. Brown, Phys. Rev. C **46**, 923 (1992).

[18] S. C. Pieper and R. B. Wiringa, Annu. Rev. Nucl. Part. Sci. **51**, 53 (2001).
[19] R. B. Wiringa (private communication). The configuration and momentum space overlaps are available at [http://www.phy.anl.gov/theory/research/overlap/].
[20] K. Arai, P. Descouvemont, D. Baye, and W. N. Catford, Phys. Rev. C **68**, 014310 (2003).
[21] K. Arai (private communication). These overlaps of Fig. 4(a) of Ref. [20] were provided with shell-model spin couplings.
[22] B. A. Brown, Phys. Rev. C **58**, 220 (1998).
[23] J. A. Tostevin, G. Podolyák, B. A. Brown, and P. G. Hansen, Phys. Rev. C **70**, 064602 (2004); J. A. Tostevin and B. A. Brown, *ibid.* **74**, 064604 (2006).
[24] S. Raman, C. H. Malarkey, W. T. Milner, C. W. Nestor Jr., and P. H. Stelson, At. Data Nucl. Data Tables **36**, 1 (1987).
[25] B. A. Brown and W. A. Richter, Phys. Rev. C **74**, 034315 (2006).
[26] A. Gade *et al.*, Phys. Rev. C **77**, 044306 (2008).
[27] E. K. Warburton, J. A. Becker, and B. A. Brown, Phys. Rev. C **41**, 1147 (1990).